Virtual unenhanced imaging of the liver derived from 160-mm rapid-switching dual-energy CT (rsDECT): Comparison of the accuracy of attenuation values and solid liver lesion conspicuity with native unenhanced images

Maxime Lacroix, Sébastien Mulé, Edouard Herin, Frédéric Pigneur, Philippe Richard, Benhalima Zegai, Laurence Baranes, Marjan Djabbari, Francesco Brunetti, Nicola De'angelis, et al.

Virtual unenhanced imaging of the liver derived from 160-mm rapid-switching dual-energy CT (rsDECT): Comparison of the accuracy of attenuation values and solid liver lesion conspicuity with native unenhanced images

Maxime Lacroix[1], Sébastien Mulé[1,2,3], Edouard Herin[1], Frédéric Pigneur[1], Philippe Richard[4], Benhalima Zegai[1], Laurence Baranes[1], Marjan Djabbari[1], Francesco Brunetti[5], Nicola de'Angelis[2,5], Alexis Laurent[2,5], Vania Tacher[1], Hicham Kobeiter[1,2], Alain Luciani[1,2,3]

[1] Service d'Imagerie Médicale, AP-HP, Hôpitaux Universitaires Henri Mondor, 94010 Créteil, France

[2] Faculté de Médecine de Créteil, Université Paris Est Créteil, 94000 Créteil, France

[3] INSERM IMRB, U 955, Equipe 18, Créteil, France

[4] GE Healthcare, 283 rue de la Minière, 78530 Buc, France

[5] Service de chirurgie digestive, AP-HP, Hôpital Henri Mondor, 94010 Créteil, France

Corresponding author: Maxime Lacroix, Service d'Imagerie Médicale, AP-HP, Hôpitaux Universitaires Henri Mondor, 51 Avenue du Marechal de Lattre de Tassigny, 94010 Créteil Cedex, France; e-mail: m.lacroix@outlook.fr ; tel: +33149812631 ; fax: +33149812632

Virtual unenhanced imaging of the liver derived from 160-mm rapid-switching dual-energy CT (rsDECT): Comparison of the accuracy of attenuation values and solid liver lesion conspicuity with native unenhanced images

Abstract

Objectives: To evaluate the reliability of attenuation values of the liver parenchyma and focal liver lesions on virtual unenhanced images from arterial (VUEart) and portal venous phases (VUEport) compared to native unenhanced (NU) attenuation values in patients referred for assessment of malignant liver lesions. *Methods*: Seventy-three patients with confirmed primary or metastatic liver tumors who underwent a multiphase contrast-enhanced rapid-switching kVp dual-energy CT (rsDECT) were included in this IRB-approved retrospective study. Both qualitative and quantitative analyses – including the lesion-to-liver contrast-to-noise ratio (LL-CNR) - were performed and compared between NU and both VUEart and VUEport images. *Results*: The mean liver attenuation values were significantly lower in VUEart images (56.7±6.7 HU) than in NU images (59.6±7.5 HU, p=0.008), and were comparable between VUEart and VUEport images (57.9±6 UH, p=0.38) and between VUEport and NU images (p=0.051). The mean liver lesions attenuation values were comparable between NU, VUEart and VUEport images (p=0.60). Strong and significant correlations values were found both in liver lesions and tumor-free parenchyma (r=0.82-0.91, p<0.01). The mean LL-CNR was significantly higher in VUEart and VUEport images than in NU images (1.7±1 and 1.6±1.1 vs 0.9±0.6; p<0.001), but was comparable between VUEart and VUEport images (p>0.9). Lesion conspicuity was significantly higher in VUEport images than in NU images (p<0.001). *Conclusion:* VUEport images derived from 3rd generation rsDECT could confidently replace NU images in patients undergoing assessment for malignant liver lesions. These images provide comparable attenuation values in both liver lesions and liver parenchyma while reducing the radiation dose and scanning time.

Key words:

Dual energy CT, Liver lesions, Virtual unenhanced, Conventional unenhanced, Image quality

Abbreviations:

NU, Native Unenhanced; VUEart, Virtual Unenhanced images from Arterial phase; VUEport, Virtual Unenhanced images from Portal phase; rsDECT, rapid-switching Dual Energy CT; IRB, Institutional Review Board; LL-CNR, Lesion-to-liver Contrast-to-noise Ratio; DECT, Dual Energy CT; HU, Hounsfield Unit; GIST, Gastro-intestinal Stromal Tumor; HCC, Hepatocellular Carcinoma; BMI, Body Mass Index; ASIR-V, Adaptive Statistical Iterative Reconstruction V; ROI, Region Of Interest; SD, Standard Deviation; DLP, Dose-Length Product; CTDI, Computed Tomography Dose Index ; TACE, Transarterial Chemoembolization; GSI, Gemstone Spectral Imaging.

1. Introduction

Dual-energy CT (DECT) is an imaging technique that allows the evaluation of tissue densities using two different X-ray energy levels. The attenuation changes observed at these two distinct energy levels vary according to the tissue atomic number, allowing DECT to optimize tissue characterization [1,2]. Several techniques are currently available to generate these two distinct energy spectra: some rely on dual-layer detector designs [3,4], while some rely on the emission of two distinct X-ray spectra including dual-source DECT or rapid-switching DECT (rsDECT) [5]. In the latter, optimized temporal registration is achieved via rapid kVp changes on emission. Third-generation rsDECT are routinely being used, especially for abdominal examinations, allowing better characterization of lesion enhancement [6,7]. In addition, rsDECT can create virtual noncontrast images derived from postcontrast series images by two distinct means. A two-material decomposition strategy can be used to generate a "material density image" reflecting the relative iodine to water content within each voxel, but this approach provides images for which Hounsfield units (HU) are no longer valid. An alternative approach with rsDECT relies on the generation of mono-energetic 70 keV images in which iodine is additionally subtracted from each voxel [8] thereby creating material-suppressed iodine images also called "virtual unenhanced images" (VUE images) [9–11]. In contrast to material density images, such VUE images allow HU quantification, with potentially easier integration in clinical practice.

Native unenhanced (NU) images are widely used in abdominal imaging both in emergency settings [12] and in oncology [13]. In liver tumor imaging, knowledge of precontrast attenuation values of tumors allows the identification of blood products, fat sparing and calcifications in tumors. It also enables accurate assessment of tumor enhancement after contrast media injection, which is of paramount importance in patients with cirrhosis and also in patients with hypervascular liver metastases because it significantly improves the lesion detection rate (13). In treated liver lesions, NU images may help in the evaluation of the response to treatment, such as with tyrosine kinase inhibitor treatment for GIST [14]. Replacing NU images with VUE images in multiphasic liver CT exams may provide several benefits including potential X-ray exposure dose reduction, reduced scanning time and reduced differences in coregistration between the NU and enhanced phases images [15–17].

To confidently replace NU images with VUE images, their comparative quality must be addressed. Previous studies have investigated the accuracy of virtual noncontrast attenuation values based on dsDECT techniques [18–21]. All of these studies showed good approximations of NU attenuation values, even if the attenuation values on virtual noncontrast images were significantly higher than those obtained with NU images. Similar reports have been made with single source dual-energy CT devices. However, the quality of VUE images for liver tumor assessment has not yet been specifically studied [22,23].

The aim of this retrospective study was to evaluate the reliability of HU attenuation values of the liver parenchyma and focal liver lesions on both arterial and portal phase-derived VUE images and compared them to NU attenuation values acquired on a 160-mm 3rd generation rsDECT in consecutive patients referred for malignant liver lesion detection or follow up.

2. Materials and methods

2.1. Population

For this institutional review board (IRB)-approved retrospective study, we identified all patients with histories of confirmed primary or metastatic liver tumors who underwent a multiphase contrast-enhanced rsDECT from May to September 2017 in our center using our local Pictorial Archive and Communication System (Carestream 3.2., Carestream Health, Rochester, New York). Written consent of the patients was waived by the IRB due to the retrospective design of the study.

Seventy-seven patients were eligible for this study. Four patients were excluded because of the absence of an arterial phase acquisition. As a result, the final population consisted of 73 patients (57 men and 16 women) aged from 32 to 86 years (mean age, 64.4 years; SD, 11.7 years). The mean body mass was 24.2 kg/m^2 ± 4.8 (range, 16.7-47.2). All patients were referred either for characterization of a liver lesion (n=5) or for follow-up under adjuvant treatment (n=68).

The final diagnosis of a primary or metastatic liver tumor was determined as follows:

- Patients with HCC (n=44) were diagnosed either using the EASL 2018 criteria [24] (n=20) or by pathology (percutaneous liver biopsy, n=4; liver resection, n=20).
- All patients with cholangiocarcinoma (n=8) or neuroendocrine metastatic disease (n=4) had their diagnoses confirmed by pathology either through surgery (n=7) or biopsy (n=5).
- The primary tumor sites in the remaining patients with metastatic lesions (n=17) were defined based on the pathological confirmation of the primary tumor and on the follow-up imaging.

The characteristics and distribution of primary and metastatic liver tumors in the 73 patients are shown in Table 1.

2.2. CT protocol

All patients underwent a multiphase abdominal contrast-enhanced DECT using a 160-mm 3rd generation rsDECT (Revolution CT; GE Healthcare, Waukesha - WI, USA). First, a NU low-dose CT scan of the abdomen was acquired (120 kVp, collimation 40 mm, pitch 1.375,

rotation 0.7 s) from the dome of the liver to the iliac crest within one breath hold. Raw data were reconstructed with an Adaptive Statistical Iterative Reconstruction V (ASIR-V) of 60% and a slice thickness/interval of 1.25/1.25 (Table 2) [25]. Then, 1.5 cc/kg of nonionic contrast medium (iomeprol, 350 mg iodine/mL; Iomeron 350, Bracco Imaging, Milano, Italy or iobitridol, 350 mg iodine/mL, Xenetix 350, Guerbet, Paris, France) was injected intravenously through a power injector at a rate of 4–5 mL/sec to acquire a contrast-enhanced arterial and portal venous phase DECT. The late arterial phase acquisition was launched 20 seconds after the attenuation increase in the abdominal aorta reached the predefined threshold of 100 HU (Smartprep, GE Healthcare, Waukesha – WI, USA), while the portal venous phase was launched 60 seconds after. The late arterial and portal venous phase images were acquired in dual-energy mode with rapid kVp-switching between 80 and 140 kVp (tube current-time 277 mAs, collimation 80 mm, pitch 0.992, and rotation 0.8 s). Arterial and portal phase-derived VUE images (VUEart and VUEport images, respectively) were reconstructed with an ASIR-V of 60% and a slice thickness/interval of 1.25/1.25.

2.3. DECT quantitative analysis

One author [M.L.] with 3 years of experience in abdominal radiology performed all quantitative analyses. All image analyses were carried out on the Carestream PACS system (Carestream 3.2., Carestream Health, Rochester, New-York). All regions of interest (ROIs) were manually positioned on the NU images as described below and then copy/pasted on VUE images.

2.3.1 Liver parenchyma and muscle analysis

For each patient, three circular ROIs were manually placed in the liver (one in the right lobe, one specifically in the quadrate lobe and one in the left lobe) in a homogeneous region, avoiding vascular structures and focal lesions (*Fig 1*). In cases of partial hepatic resection (hepatectomy or lobectomy), the ROIs were positioned evenly in the remaining parenchyma.
In addition, one circular ROI was positioned in each erector spinae muscle at the level of the vertebral body of L1. The mean size of the liver and muscle ROIs was 250 ± 12.5 mm^2 and 150 ± 10.1 mm^2, respectively.

2.3.2 Liver tumor analysis

Quantitative analysis of attenuation values was performed only in supracentimetric liver tumors. For each patient, 2 radiologists (reader 1 [A.L] and reader 2 [M.L.] with 15 and 3 years of experience in abdominal radiology, respectively) separately reviewed all image sets. Both readers manually positioned circular ROIs on the two largest supracentimetric lesions detected. All ROIs were then copy/pasted on the corresponding VUEart and VUEport images. The mean ROI size was 250 ± 24.3 mm^2. The mean density value and the corresponding standard deviation (SD) were measured in the liver, the muscles and the liver lesions. The lesion-to-liver contrast-to-noise ratio (LL-CNR) was computed as follows:

Equation 1:

$$LL - CNR = \frac{|HU_{lesion} - HU_{liver}|}{SD_{liver}}$$

where HU_{lesion} and HU_{liver} are the mean density values of the liver lesion and the liver parenchyma, respectively, while SD_{liver} is the mean standard deviation of the liver density values.

2.4. DECT qualitative analysis

Image quality was indirectly assessed by evaluating lesion conspicuity and detectability.

2.4.1 Lesion conspicuity

Qualitative analysis of the supracentimetric lesions previously segmented was additionally performed on the NU, VUEart and VUEport images using a 4-point scale (4 <best>: nodule with clearly defined edges, 3: nodule with some imprecise edges, 2: nodule likely visible, 1 <worst>: nodule not visible).

The same two radiologists separately determined the lesion conspicuity for each lesion. A subjective image quality score ≥ 3 was considered good. The analysis was also performed by separating the hypervascular and nonhypervascular lesions. Hypervascular lesions were defined by nonrim-like enhancement in that arterial phase that was unequivocally greater in whole or in part than the liver [26].

2.4.2 Lesion detectability

Detectability of the lesions was assessed by counting the number of all tumor nodules detectable on the NU, VUEart and VUEport images, irrespective of their size.
Combined analysis of both unenhanced and contrast-enhanced arterial and portal venous phase images was performed to determine the global number of malignant lesions for each patient.

2.5. Radiation dose

Radiation exposure was investigated: the total dose-length product (DLP, mGy.cm) value was systematically collected, and the specific values of the DLP and CTDI for the NU, arterial and portal venous phase images were also collected.

2.6. Statistical analysis

Variables were assessed for normality by using the Kolmogorov Smirnov test. The mean density values of the liver, muscle and lesions and the LL-CNR were measured on NU, VUEart and VUEport images, and the respective DLP and $CTDI_{vol}$ were compared using Kruskal Wallis and Dunn's multiple comparison tests. An overall significance level of 0.05 was used for each hypothesis. Pearson correlation test was used to evaluate correlation between NU, VUEart and VUEport attenuation values. The interobserver agreement of lesion conspicuity was determined using Cohen's kappa coefficient. All statistical analyses were performed using MedCalc® software (version 12.2.1.0).

3. Results

3.1. Quantitative analysis

Table 3 summarizes the mean attenuation values of the liver, muscles and liver lesions as well as the LL-CNR measured on the NU, VUEart and VUEport images for the 73 patients.

The mean attenuation values of the liver were significantly lower in VUEart images (56.7±6.7 HU) than in NU images (59.6±7.5 HU), p=0.008. There was no difference in the mean liver attenuation values between VUEart and VUEport images (57.9±6 HU; p=0.38) or between VUEport and NU images (p=0.051) *(Fig 2A)*.

Mean NU attenuation values in the liver significantly correlated with VUEart and VUEport ones (r=0.90, p<0.001; r=0.91, p<0.001 respectively). A strong correlation was also found between mean VUEart and VUEport attenuation values in the liver (r=0.90, p<0.001).

The mean attenuation values of the muscles were significantly higher in NU images (51.8±5.2 HU) than in VUEart (47.1±5.4 HU) and VUEport images (48.4±5.3 HU), p<0.0001. There was no difference in the muscle attenuation values between VUEart and VUEport images (p=0.17) *(Fig 2B)*.

A lower but significant correlation was found between mean NU muscle attenuation values and both mean VUEart and VUEport muscle attenuation values (r=0.72, p<0.001; r=0.79, p<0.001 respectively), and between mean VUEart and VUEport muscle attenuation values (r=0.76, p<0.001).

A total of 52 supracentimetric lesions were selected for the liver tumor analysis.

The mean attenuation values of liver lesions were not significantly different among the NU, VUEart and VUEport images (liver lesions attenuation values of 41.6±8.6 HU, 39.7±9.6 HU and 41±10.3 HU, respectively; p=0.60).

Mean NU attenuation values in liver lesions significantly correlated with mean VUEart and VUEport ones (r=0.83, p<0.001; r=0.80, p<0.001 respectively). Mean VUEart and VUEport attenuations values in liver lesions were also significantly correlated (r=0.88, p<0.001)

Thirty-eight out of 52 (73%) liver lesions were nonhypervascular, and 14 out of 52 (27%) were hypervascular. Most of hypervascular lesions were HCC (12/14, 85.7%), and the most

frequent histological types among nonhypervascular lesions were colorectal cancer metastasis (14/38, 36.8%) and HCC (11/38, 28.9%).

The attenuation values of nonhypervascular and hypervascular lesions were respectively of 41.3 HU and 41.4 HU on NU, 39 HU and 40.9 HU on VUEart and 39.5 HU and 42.1 HU on VUEport.

There was no difference in attenuation values between the hypervascular and the nonhypervascular lesions in NU (p= 0.77), VUEart (p= 0.62) and VUEport images (p=0.34).

There was no difference in the LL-CNR between VUEart and VUEport images (p>0.9) *(Fig 2D)*.

The mean LL-CNR was significantly higher in VUEart (1.7±1) and VUEport images (1.6±1.1) than in NU images (0.9±0.6), p<0.001 (Fig 3).

3.2. Qualitative analysis

3.2.1. Lesion conspicuity

Lesion conspicuity was classified as good (score 3 or 4) for readers 1 and 2 in 52% and 44% of NU images, respectively, 73% and 67% of VUEart images, respectively, and 90% and 96% of VUEport images, respectively (Table 4). Lesion conspicuity (using a 4-point scale) was significantly higher on VUEport images than on NU images for both readers (p<0.001), significantly higher on VUEart images than on NU images (p=0.03 for reader 1 and p=0.01 for reader 2), and significantly higher on VUEport images than on VUEart images (p<0.001 for both readers) (*Fig 4*).

The image conspicuity of nonhypervascular lesions was significantly better than that of hypervascular lesions in VUEart images for both readers (p=0.001 for reader 1 and 0.01 for reader 2), while there was no significance difference between hypervascular and nonhypervascular lesions for both readers on NU and VUEport images (Table 5).

Inter-reader agreement regarding the lesion conspicuity assessment was moderate for the NU images (k=0.55), good for the VUEart images (k=0.64), and excellent for the VUEport images (k=0.93).

3.2.2. Lesion detectability

Based on the reference standard, a total of 386 lesions were detected combining the different series. VUEport images allowed the detection of significantly more lesions (332/386: 86%) than both VUEart images (304/386: 78%, p=0.008) and NU images (165/386: 42%, p<0.001). NU images allowed the detection of significantly fewer lesions than VUEart images (p<0.001).

3.3. Radiation Dose

The mean total DLP was 2007±530 mGy.cm. The specific mean CTDI of the NU, arterial and portal venous phase images were 7.5±2.8, 15.8±4.8 and 14.3±3.8 mGy, respectively, accounting for 20%, 42% and 38% of the total $CTDI_{vol}$, respectively.
The specific DLP of the NU, arterial and portal venous phase images were 234±104, 701±227 and 849±233 mGy.cm, respectively (Table 6).

4. Discussion

Our results show that VUEport-derived attenuation values were comparable to NU attenuation values both in focal liver lesions and in the liver parenchyma. Moreover, lesion conspicuity on VUEport images was increased when compared to NU low-dose images, suggesting that VUEport images could confidently replace NU images during contrast-enhanced CT follow-up on a 3rd generation rsDECT in patients with malignant liver lesions.

NU images are required in everyday practice to analyze and characterize liver tumors. They allow accurately appreciation of tumor enhancement after contrast media injection both in hypervascular and nonhypervascular liver lesions, particularly after therapy [24,27] [28–32].

Two previous studies using rsDECT compared the reliability of liver VUE images compared with NU images [22,23]. Borhani et al. reported significant differences in the mean attenuation values observed in NU and VUE images within the muscles, reaching up to 5.9 HU mean differences on VUE arterial images [22], which are similar to those of our study.

Interestingly, these authors reported a significant number of cases in which individual errors were higher than 10 HU, which are differences that we did not encounter in our study. Differences in liver attenuation values between NU and VUEart images were not significant in Mahmood et al.'s study [23]. Interestingly, the authors performed NU acquisition with a different acquisition protocol than in our study. Additionally, VUE and NU images were only compared using VUE images derived from arterial phase imaging. Last, the acquisition was not performed on the same CT platform as in this study, suggesting that the reconstruction algorithms used in rsDECT platforms differ between CT generations. In addition, our findings further show that the mean attenuation values observed within the liver, the muscles and the liver lesions were not significantly different when comparing VUEart and VUEport images, which is a finding not reported to date.

In our study, there was no difference in attenuation values between the hypervascular and the nonhypervascular lesions on both NU and VUE images.

We found significant correlation values between NU, VUEart and VUEport attenuation values in both liver lesions and liver tumor-free parenchyma, in agreement with previous studies using rapid-switching DECT [22]. Correlation values were moderate in paraspinal muscles, in line with previously published ones. [21,22]

Previous studies using dsDECT demonstrated that the mean LL-CNR was significantly higher in arterial- and portal-derived VUE images than in NU images, without differences between arterial- and portal-derived VUE images [21,33,34], which are similar results to our findings. One study found similar noise levels between NU and VUE images [35]. To our knowledge, our study is the first to show these results with a 3rd generation rsDECT for liver tumors.

In our study, the subjective quality (conspicuity and detectability) of VUEport images was ranked higher than that of VUEart or NU images, without a significant difference between VUEart and NU images. Similar findings were already suggested by Mahmood et al [23]. Conflicting results have been reported regarding liver lesion conspicuity, especially in studies dealing with dual-source DECT: some authors subjectively considered the conventional unenhanced series to be of higher quality than portal and arterial VUE images [20,33]. This was attributed either to reader preference or to the fact that they were more used to seeing the

conventional unenhanced images in day-to-day practice. No significant difference in mean image quality was recorded in another study [21].

In our study, there was no difference in attenuation values between the hypervascular and the nonhypervascular lesions on both NU and VUEport images. However, the image conspicuity of nonhypervascular lesions was significantly better than that of hypervascular lesions on VUEart for both readers. This could be attributed to a suboptimal suppression of high iodine content of hypervascular lesions, as opposed to moderate iodine content within nonhypervascular lesions.
Our study shows that VUEport images provide accurate detectability of liver lesions, particularly compared to NU images. This is an important point, as noncontrast phase images have been shown to improve the detection of hypervascular liver metastases [13].

While attenuation values from NU images only depend on tissues intrinsic characteristics, attenuation values from VUE images are post-processed data sets created by the removal of the iodine component in each pixel using iodine-water decomposition. This mathematical operation may be inaccurate as iodine concentration is highly dependent on both intrinsic and extrinsic examination parameters such as Body Mass Index (BMI), cardiovascular status [36] or the tissue vasculature [37]. Air, organ boundaries and artifacts from hyper-attenuating regions could also lead to misestimation of iodine concentration values within tumors [38].

Substantial radiation dose savings are possible if VUE image reconstructions replace NU images [35]. In our cohort, the suppression of NU images could have led to a mean reduction of approximately 20% of the total CT dose. This dose reduction is lower than what has been suggested by previous studies, with an expected dose reduction ranging from 24.8 to 35.1% [21,23,34,35,39–42]. This could in part be explained by the fact that the acquisition parameters of the NU series in our study were optimized with a mean CTDI close to 7 mGy, in agreement with our radiation dose national recommendations [43].

Our study has some limitations. First, this retrospective study included a small number of patients, which did not allow us to perform subgroup analysis based on underlying liver diseases such as liver steatosis or cirrhosis. Although we did not encounter this specific issue

in our study population, the detectability of liver lesions may prove defective in images with stones/calcifications, hemorrhages, and fat lesions as reported by Mahmood et al. [23]. In addition, the behavior of VUE images in the presence of lipiodol has not been assessed in this study. Potential lipiodol subtraction by VUE reconstruction algorithms would hamper the quantification of lipiodol uptake following transarterial chemoembolization (TACE) although this feature is a known prognostic marker of TACE efficiency.

Finally, the lower conspicuity and detection rate on the unenhanced images may be due to the low-dose protocol of this acquisition. Nevertheless, in everyday practice, low-dose unenhanced acquisitions are widely prevalent, explaining our choice to assess these types of acquisitions.

5. Conclusion:

VUEport images derived from 3rd generation rsDECT could confidently replace NU images during contrast-enhanced CT follow-up in patients with malignant liver lesions. These images provide comparable attenuation values both in focal liver lesions and in the liver parenchyma while reducing radiation dose and scanning time.

This research did not receive any specific grant from funding agencies in the public, commercial, or not-for-profit sectors.

References:

[1] H.W. Goo, J.M. Goo, Dual-Energy CT: New Horizon in Medical Imaging, Korean J. Radiol. 18 (2017) 555. https://doi.org/10.3348/kjr.2017.18.4.555.
[2] T.R.C. Johnson, Dual-Energy CT: General Principles, Am. J. Roentgenol. 199 (2012) S3–S8. https://doi.org/10.2214/AJR.12.9116.
[3] N.E. Atwi, D.L. Smith, C.D. Flores, E. Dharaiya, R. Danrad, A. Kambadakone, A.M. Toshav, Dual-energy CT in the obese: a preliminary retrospective review to evaluate quality and feasibility of the single-source dual-detector implementation, Abdom. Radiol. 44 (2019) 783–789. https://doi.org/10.1007/s00261-018-1774-y.
[4] X.-M. Zhao, M. Wang, R.-Z. Wu, E. Dharaiya, F. Feng, M.-L. Li, H. You, Y. Wang, Y.-N. Wang, Z.-Y. Jin, Dual-layer spectral detector CT monoenergetic reconstruction improves image quality of non-contrast cerebral CT as compared with conventional single energy CT, Eur. J. Radiol. 103 (2018) 131–138. https://doi.org/10.1016/j.ejrad.2018.04.015.
[5] T. Sellerer, P.B. Noël, M. Patino, A. Parakh, S. Ehn, S. Zeiter, J.A. Holz, J. Hammel, A.A. Fingerle, F. Pfeiffer, D. Maintz, E.J. Rummeny, D. Muenzel, D.V. Sahani, Dual-energy CT: a phantom comparison of different platforms for abdominal imaging, Eur. Radiol. 28 (2018) 2745–2755. https://doi.org/10.1007/s00330-017-5238-5.
[6] A. Graser, T.R.C. Johnson, H. Chandarana, M. Macari, Dual energy CT: preliminary observations and potential clinical applications in the abdomen, Eur. Radiol. 19 (2009) 13–23. https://doi.org/10.1007/s00330-008-1122-7.
[7] A. Euler, J. Solomon, M.A. Mazurowski, E. Samei, R.C. Nelson, How accurate and precise are CT based measurements of iodine concentration? A comparison of the minimum detectable concentration difference among single source and dual source dual energy CT in a phantom study, Eur. Radiol. 29 (2019) 2069–2078. https://doi.org/10.1007/s00330-018-5736-0.
[8] Y. Chai, J. Xing, J. Gao, P. Lv, P. Liang, J. Liu, Y. Guo, Feasibility of virtual nonenhanced images derived from single-source fast kVp-switching dual-energy CT in evaluating gastric tumors, Eur. J. Radiol. 85 (2016) 366–372. https://doi.org/10.1016/j.ejrad.2015.11.015.
[9] M. Petersilka, H. Bruder, B. Krauss, K. Stierstorfer, T.G. Flohr, Technical principles of dual source CT, Eur. J. Radiol. 68 (2008) 362–368. https://doi.org/10.1016/j.ejrad.2008.08.013.
[10] T. Lestra, S. Mulé, I. Millet, A. Carsin-Vu, P. Taourel, C. Hoeffel, Applications of dual energy computed tomography in abdominal imaging, Diagn. Interv. Imaging. 97 (2016) 593–603. https://doi.org/10.1016/j.diii.2015.11.018.
[11] A.C. Silva, B.G. Morse, A.K. Hara, R.G. Paden, N. Hongo, W. Pavlicek, Dual-Energy (Spectral) CT: Applications in Abdominal Imaging, RadioGraphics. 31 (2011) 1031–1046. https://doi.org/10.1148/rg.314105159.
[12] Y. Geffroy, I. Boulay-Coletta, M.-C. Jullès, S. Nakache, P. Taourel, M. Zins, Increased Unenhanced Bowel-Wall Attenuation at Multidetector CT Is Highly Specific of Ischemia Complicating Small-Bowel Obstruction, Radiology. 270 (2014) 159–167. https://doi.org/10.1148/radiol.13122654.
[13] J.H. Oliver, R.L. Baron, M.P. Federle, B.C. Jones, R. Sheng, Hypervascular liver metastases: do unenhanced and hepatic arterial phase CT images affect tumor detection?, Radiology. 205 (1997) 709–715. https://doi.org/10.1148/radiology.205.3.9393525.

[14] R.S. Benjamin, H. Choi, H.A. Macapinlac, M.A. Burgess, S.R. Patel, L.L. Chen, D.A. Podoloff, C. Charnsangavej, We Should Desist Using RECIST, at Least in GIST, J. Clin. Oncol. 25 (2007) 1760–1764. https://doi.org/10.1200/JCO.2006.07.3411.
[15] Y. Nagayama, A. Iyama, S. Oda, N. Taguchi, T. Nakaura, D. Utsunomiya, Y. Kikuchi, Y. Yamashita, Dual-layer dual-energy computed tomography for the assessment of hypovascular hepatic metastases: impact of closing k-edge on image quality and lesion detectability, Eur. Radiol. 29 (2019) 2837–2847. https://doi.org/10.1007/s00330-018-5789-0.
[16] S.S. Martin, F. Trapp, J.L. Wichmann, M.H. Albrecht, L. Lenga, J. Durden, C. Booz, T.J. Vogl, T. D'Angelo, Dual-energy CT in early acute pancreatitis: improved detection using iodine quantification, Eur. Radiol. 29 (2019) 2226–2232. https://doi.org/10.1007/s00330-018-5844-x.
[17] P. Lv, X. Lin, J. Gao, K. Chen, Spectral CT: Preliminary Studies in the Liver Cirrhosis, Korean J. Radiol. 13 (2012) 434. https://doi.org/10.3348/kjr.2012.13.4.434.
[18] S. Kaufmann, A. Sauter, D. Spira, S. Gatidis, D. Ketelsen, M. Heuschmid, C.D. Claussen, C. Thomas, Tin-filter Enhanced Dual-Energy-CT, Acad. Radiol. 20 (2013) 596–603. https://doi.org/10.1016/j.acra.2013.01.010.
[19] H.A. Lee, Y.H. Lee, K.-H. Yoon, D.-H. Bang, D.E. Park, Comparison of Virtual Unenhanced Images Derived From Dual-Energy CT With True Unenhanced Images in Evaluation of Gallstone Disease, Am. J. Roentgenol. 206 (2016) 74–80. https://doi.org/10.2214/AJR.15.14570.
[20] V.A. Sahni, A.B. Shinagare, S.G. Silverman, Virtual unenhanced CT images acquired from dual-energy CT urography: Accuracy of attenuation values and variation with contrast material phase, Clin. Radiol. 68 (2013) 264–271. https://doi.org/10.1016/j.crad.2012.08.004.
[21] C.N. De Cecco, V. Buffa, S. Fedeli, M. Luzietti, A. Vallone, R. Ruopoli, V. Miele, M. Rengo, P. Paolantonio, M. Maurizi Enrici, A. Laghi, V. David, Dual energy CT (DECT) of the liver: conventional versus virtual unenhanced images, Eur. Radiol. 20 (2010) 2870–2875. https://doi.org/10.1007/s00330-010-1874-8.
[22] A.A. Borhani, M. Kulzer, N. Iranpour, A. Ghodadra, M. Sparrow, A. Furlan, M.E. Tublin, Comparison of true unenhanced and virtual unenhanced (VUE) attenuation values in abdominopelvic single-source rapid kilovoltage-switching spectral CT, Abdom. Radiol. 42 (2017) 710–717. https://doi.org/10.1007/s00261-016-0991-5.
[23] U. Mahmood, N. Horvat, J.V. Horvat, D. Ryan, Y. Gao, G. Carollo, R. DeOcampo, R.K. Do, S. Katz, S. Gerst, C.R. Schmidtlein, L. Dauer, Y. Erdi, L. Mannelli, Rapid switching kVp dual energy CT: Value of reconstructed dual energy CT images and organ dose assessment in multiphasic liver CT exams, Eur. J. Radiol. 102 (2018) 102–108. https://doi.org/10.1016/j.ejrad.2018.02.022.
[24] P.R. Galle, A. Forner, J.M. Llovet, V. Mazzaferro, F. Piscaglia, J.-L. Raoul, P. Schirmacher, V. Vilgrain, EASL Clinical Practice Guidelines: Management of hepatocellular carcinoma, J. Hepatol. 69 (2018) 182–236. https://doi.org/10.1016/j.jhep.2018.03.019.
[25] P. De Marco, D. Origgi, New adaptive statistical iterative reconstruction ASiR-V: Assessment of noise performance in comparison to ASiR, J. Appl. Clin. Med. Phys. 19 (2018) 275–286. https://doi.org/10.1002/acm2.12253.
[26] A. Tang, M.R. Bashir, M.T. Corwin, I. Cruite, C.F. Dietrich, R.K.G. Do, E.C. Ehman, K.J. Fowler, H.K. Hussain, R.C. Jha, A.R. Karam, A. Mamidipalli, R.M. Marks, D.G. Mitchell, T.A.

Morgan, M.A. Ohliger, A. Shah, K.-N. Vu, C.B. Sirlin, For the LI-RADS Evidence Working Group, Evidence Supporting LI-RADS Major Features for CT- and MR Imaging–based Diagnosis of Hepatocellular Carcinoma: A Systematic Review, Radiology. 286 (2018) 29–48. https://doi.org/10.1148/radiol.2017170554.
[27] M. Ronot, F. Cuccioli, M. Dioguardi Burgio, M.-P. Vullierme, O. Hentic, P. Ruszniewski, G. d'Assignies, V. Vilgrain, Neuroendocrine liver metastases: Vascular patterns on triple-phase MDCT are indicative of primary tumour location, Eur. J. Radiol. 89 (2017) 156–162. https://doi.org/10.1016/j.ejrad.2017.02.007.
[28] K.S. Cools, A.M. Moon, L.M.B. Burke, K.A. McGinty, P.D. Strassle, D.A. Gerber, Validation of the Liver Imaging Reporting and Data System Treatment Response Criteria After Thermal Ablation for Hepatocellular Carcinoma, Liver Transpl. (2019). https://doi.org/10.1002/lt.25673.
[29] H. Nakai, S. Arizono, H. Isoda, K. Togashi, Imaging Characteristics of Liver Metastases Overlooked at Contrast-Enhanced CT, Am. J. Roentgenol. 212 (2019) 782–787. https://doi.org/10.2214/AJR.18.20526.
[30] S.W. Kwan, N. Fidelman, E. Ma, R.K. Kerlan, F.Y. Yao, Imaging predictors of the response to transarterial chemoembolization in patients with hepatocellular carcinoma: A radiological-pathological correlation, Liver Transpl. 18 (2012) 727–736. https://doi.org/10.1002/lt.23413.
[31] S.H. Tirumani, A.D. Baheti, H. Tirumani, A. O'Neill, J.P. Jagannathan, Update on Gastrointestinal Stromal Tumors for Radiologists, Korean J. Radiol. 18 (2017) 84. https://doi.org/10.3348/kjr.2017.18.1.84.
[32] H. Choi, C. Charnsangavej, S. de C. Faria, E.P. Tamm, R.S. Benjamin, M.M. Johnson, H.A. Macapinlac, D.A. Podoloff, CT Evaluation of the Response of Gastrointestinal Stromal Tumors After Imatinib Mesylate Treatment: A Quantitative Analysis Correlated with FDG PET Findings, Am. J. Roentgenol. 183 (2004) 1619–1628. https://doi.org/10.2214/ajr.183.6.01831619.
[33] T. Barrett, D.J. Bowden, N. Shaida, E.M. Godfrey, A. Taylor, D.J. Lomas, A.S. Shaw, Virtual unenhanced second generation dual-source CT of the liver: Is it time to discard the conventional unenhanced phase?, Eur. J. Radiol. 81 (2012) 1438–1445. https://doi.org/10.1016/j.ejrad.2011.03.042.
[34] L.-J. Zhang, J. Peng, S.-Y. Wu, Z.J. Wang, X.-S. Wu, C.-S. Zhou, X.-M. Ji, G.-M. Lu, Liver virtual non-enhanced CT with dual-source, dual-energy CT: a preliminary study, Eur. Radiol. 20 (2010) 2257–2264. https://doi.org/10.1007/s00330-010-1778-7.
[35] A.S. Purysko, A.N. Primak, M.E. Baker, N.A. Obuchowski, E.M. Remer, B. John, B.R. Herts, Comparison of radiation dose and image quality from single-energy and dual-energy CT examinations in the same patients screened for hepatocellular carcinoma, Clin. Radiol. 69 (2014) e538–e544. https://doi.org/10.1016/j.crad.2014.08.021.
[36] G. Corrias, P. Sawan, U. Mahmood, J. Zheng, M. Capanu, M. Salvatore, G. Spinato, L. Saba, L. Mannelli, Dual energy computed tomography analysis in cancer patients: What factors affect iodine concentration in contrast enhanced studies?, Eur. J. Radiol. 120 (2019) 108698. https://doi.org/10.1016/j.ejrad.2019.108698.
[37] H. Yamauchi, M. Buehler, M.M. Goodsitt, N. Keshavarzi, A. Srinivasan, Dual-Energy CT–Based Differentiation of Benign Posttreatment Changes From Primary or Recurrent Malignancy of the Head and Neck: Comparison of Spectral Hounsfield Units at 40 and 70 keV and Iodine Concentration, Am. J. Roentgenol. 206 (2016) 580–587. https://doi.org/10.2214/AJR.15.14896.

[38] A. Agostini, U. Mahmood, Y. Erdi, A. Borgheresi, M. Ragucci, P. Sawan, D. Ryan, M.E. Laino, G. Corrias, L. Mannelli, Quantification of Iodine Concentration Using Single-Source Dual-Energy Computed Tomography in a Calf Liver, J. Comput. Assist. Tomogr. 42 (2018) 222–229. https://doi.org/10.1097/RCT.0000000000000685.
[39] M. Sakane, T. Kim, M. Hori, H. Onishi, A. Nakamoto, T. Tsuboyama, M. Tatsumi, N. Tomiyama, Effects of High-concentration contrast material and low-voltage CT on contrast for multiphasic CT of the upper abdomen: comparison using the simulation with virtual monochromatic imaging obtained by fast-switch kVp dual-energy CT, SpringerPlus. 3 (2014) 234. https://doi.org/10.1186/2193-1801-3-234.
[40] A. Graser, T.R.C. Johnson, E.M. Hecht, C.R. Becker, C. Leidecker, M. Staehler, C.G. Stief, H. Hildebrandt, M.C.B. Godoy, M.E. Finn, F. Stepansky, M.F. Reiser, M. Macari, Dual-Energy CT in Patients Suspected of Having Renal Masses: Can Virtual Nonenhanced Images Replace True Nonenhanced Images?, Radiology. 252 (2009) 433–440. https://doi.org/10.1148/radiol.2522080557.
[41] Y. Yamada, M. Jinzaki, Y. Tanami, T. Abe, S. Kuribayashi, Virtual Monochromatic Spectral Imaging for the Evaluation of Hypovascular Hepatic Metastases: The Optimal Monochromatic Level With Fast Kilovoltage Switching Dual-Energy Computed Tomography, Invest. Radiol. 47 (2012) 292–298. https://doi.org/10.1097/RLI.0b013e318240a874.
[42] M.M. Goodsitt, E.G. Christodoulou, S.C. Larson, Accuracies of the synthesized monochromatic CT numbers and effective atomic numbers obtained with a rapid kVp switching dual energy CT scanner: Accuracies of DECT monochromatic CT numbers and Zeff, Med. Phys. 38 (2011) 2222–2232. https://doi.org/10.1118/1.3567509.
[43] https://nrd.irsn.fr/Ressources/Documents/Decision_NRD_2019.pdf, (n.d.).

Tables:

Table 1: Patient population.

Variable	Population (n=73)
Sex	
Male (n(%))	57 (78)
Female (n(%))	16 (22)
Age (years ± SD)	67 ± 11.7
BMI (mean in kg/m² ± SD)	24.2 ± 25.4
Type of tumor (n(%))	
Patients with primary liver tumors	52 (71)
HCC	44
Cholangiocarcinoma	8
Patients with liver metastases	21 (29)
Colorectal cancer	9
Neuroendocrine tumor	4
Pancreatic adenocarcinoma cancer	2
Breast cancer	2
Gastric adenocarcinoma cancer	2
Renal cell carcinoma	1
Urinary bladder tumor	1

Table 2: rsDECT acquisition protocol.

	Abdomen NU phase	**Thorax and abdomen arterial phase with GSI**	**Abdomen and pelvis portal venous phase with GSI**
Collimation	Helical 40 mm	Helical 80 mm	Helical 80 mm
kV	120 kV	80-140 kV	80-140 kV
NI	16	16	16
Pitch	1.375	0.992	0.992
Slice Thickness/Interval	1.25/1.25	1.25/1.25	1.25/1.25
ASIR-V	60%	60%	60%

NU: Native unenhanced. GSI: Gemstone Spectral Imaging. NI: Noise Index. ASIR-V: Adaptive Statistical Iterative Reconstruction-V

Table 3: Comparison of the mean attenuation values, standard deviations and lesion-to-liver contrast-to-noise ratio (LL-CNR) measured on native unenhanced (NU) and virtual unenhanced images derived from the arterial phase (VUEart) and the portal venous phase (VUEport).

Location	**Mean attenuation value ± SD (NU)**	**Mean attenuation value ± SD (VUEart)**	**Mean attenuation value ± SD (VUEport)**	**p value***
Liver parenchyma	59.6±7.5	56.7±6.7	57.9±6	p<0.01
Erector spinae muscles	51.8±5.2	47.1±5.4	48.4±5.3	p<0.0001
Liver lesions	41.6±8.6	39.7±9.6	41±10.3	p=0.60
LL-CNR	0.9±0.6	1.7±1	1.6±1.1	p<0.001

* *p values calculated with* Kruskal-Wallis test.

Attenuation values are given in HU.

Table 4: Lesion conspicuity with a 4-point scale for the two readers on the NU, VUEart and VUEport images.

Phase	Lesion conspicuity	Reader 1 n(%)	Reader 2 n(%)
NU images	1	12 (23.1)	7 (13.4)
	2	13 (25)	22 (42.3)
	3	17 (32.7)	20 (38.5)
	4	10 (19.2)	3 (5.8)
VUEart	1	2 (3.8)	4 (7.7)
	2	12 (23.1)	13 (25)
	3	21 (40 .4)	21 (40.4)
	4	17 (32.7)	14 (26.9)
VUEport	1	2 (3.8)	2 (3.8)
	2	3 (5.8)	0
	3	7 (13.5)	32 (61.6)
	4	40 (76.9)	18 (34.6)

4: nodule with clearly defined edges, 3: nodule with some imprecise edges, 2: nodule likely visible, 1: nodule not visible.

Table 5: Comparison of conspicuity in nonhypervascular and hypervascular lesions.

Supracentimetric liver lesions (n=52)	**Conspicuity**	**Reader 1**				**Reader 2**		
		NU	VUEart	VUEport		NU	VUEart	VUEport
Nonhypervascular lesions (n=38)	1	7	1	1		4	1	1
	2	11	5	1		14	8	0
	3	11	15	5		18	17	22
	4	9	17	31		2	12	15
Hypervascular lesions (n=14)	1	5	1	1		3	3	1
	2	2	7	2		8	7	0
	3	6	6	2		2	2	10
	4	1	0	9		1	2	3
p-value (Fisher test)		0.25	0.001	0.26		0.11	0.01	0.31

Table 6: Radiation exposure.

	CTDI (mGy)	DLP (mGy.cm)
3-phase CT scan		2007
- NU acquisition	7.5	234
- Arterial phase acquisition	15.8	701
- Portal venous phase acquisition	14.3	849

Figures:

Fig. 1:

Example of ROI placement for quantitative analysis on a VUEport image. (A) Three circular ROIs were manually placed in the liver (one in the right lobe, one specifically in the quadrate lobe and one in the left lobe). (B) One circular ROI was also manually placed in each erector spinae muscle.

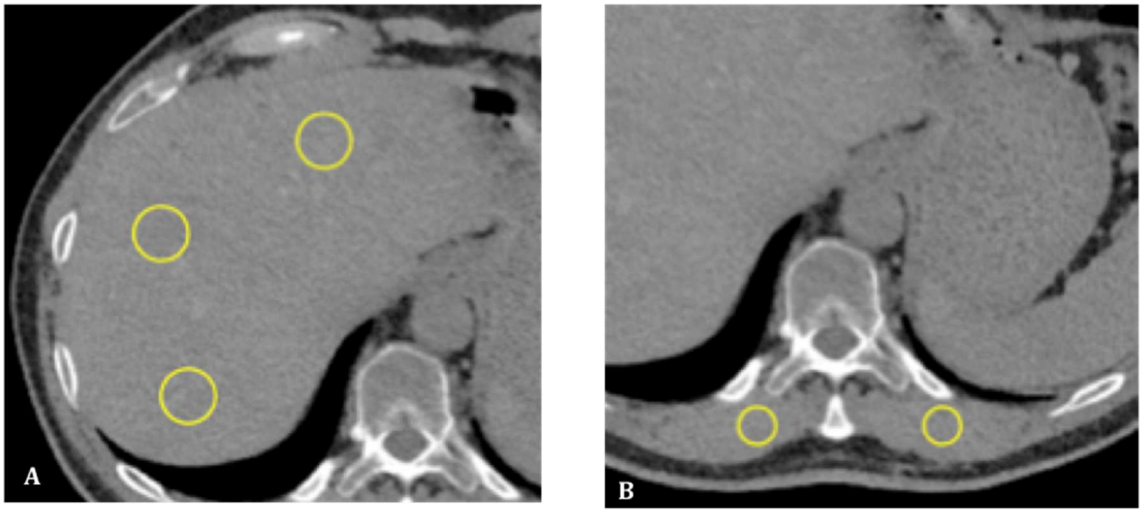

Fig. 2:

rsDECT attenuation values and the lesion-to-liver contrast-to-noise ratio (LL-CNR) on late arterial virtual unenhanced (VUEart) images and portal venous phase virtual unenhanced (VUEport) images compared to native unenhanced (NU) images. A. Comparison of the mean liver attenuation values (±SD) on NU, VUEart and VUEport images. B. Comparison of the mean muscle attenuation values (±SD) on NU, VUEart and VUEport images. C. Comparison of the standard deviation of liver attenuation values on NU, VUEart and VUEport images. D. Comparison of the mean LL-CNR in NU, VUEart and VUEport images.

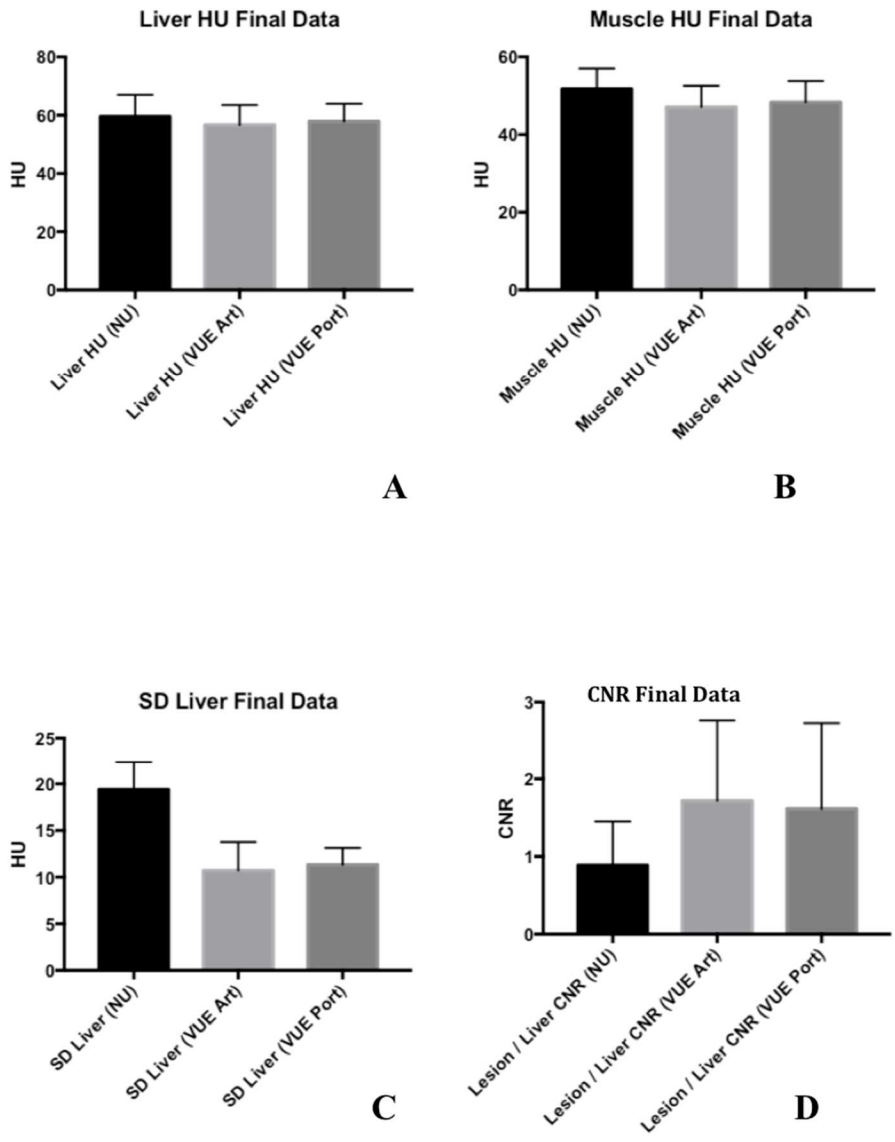

Fig. 3:

Conventional unenhanced (NU) images (A), arterial virtual unenhanced (VUEart) images (B) and portal venous phase virtual unenhanced (VUEport) images (C) in a 70 y/o woman with liver metastases of colorectal cancer. The lesion-to-liver CNR of the liver metastases in segment 6 (arrow) was significantly higher on VUEport images than on VUEart and NU images.

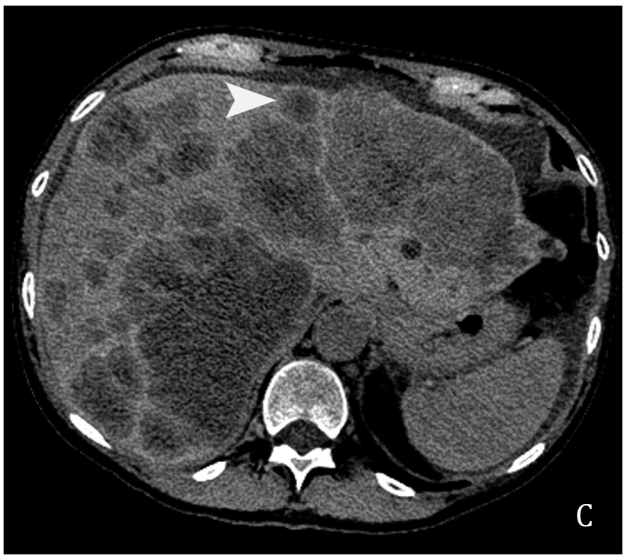

Fig. 4:

Native unenhanced (NU) images (A), arterial virtual unenhanced (VUEart) images (B) and portal venous phase virtual unenhanced (VUEport) images (C) in a 57 y/o woman with liver metastases of neuroendocrine pancreatic tumor. The lesion conspicuity was significantly higher on VUEport images than on VUEart and NU images (arrowhead).